NEUROSCIENCE

Ectopic expression of *Irx3* and *Irx5* in the paraventricular nucleus of the hypothalamus contributes to defects in *Sim1* haploinsufficiency

Joe Eun Son[1]*, Zhengchao Dou[1,2], Siyi Wanggou[1,3,4], Jade Chan[1,2], Rong Mo[1], Xuejun Li[3,4], Xi Huang[1,2], Kyoung-Han Kim[1†], Jacques L. Michaud[5,6], Chi-chung Hui[1,2]*

The paraventricular nucleus of the hypothalamus (PVH) contains a heterogeneous cluster of *Sim1*-expressing neurons critical for feeding regulation. *Sim1* haploinsufficiency results in hyperphagic obesity with disruption of PVH neurons, yet the molecular profiles of PVH neurons and the mechanism underlying the defects of *Sim1* haploinsufficiency are not well understood. By single-cell RNA sequencing, we identified two major populations of *Sim1*$^+$ PVH neurons, which are differentially affected by *Sim1* haploinsufficiency. The *Iroquois* homeobox genes *Irx3* and *Irx5* have been implicated in the hypothalamic control of energy homeostasis. We found that *Irx3* and *Irx5* are ectopically expressed in the *Sim1*$^+$ PVH cells of *Sim1*$^{+/-}$ mice. By reducing their dosage and PVH-specific deletion of *Irx3*, we demonstrate that misexpression of *Irx3* and *Irx5* contributes to the defects of *Sim1*$^{+/-}$ mice. Our results illustrate abnormal hypothalamic activities of *Irx3* and *Irx5* as a central mechanism disrupting PVH development and feeding regulation in *Sim1* haploinsufficiency.

INTRODUCTION

The paraventricular nucleus of the hypothalamus (PVH) is a complex brain region consisting of a highly heterogeneous population of neurons with diverse physiological functions including appetite regulation (*1*–*3*). In the mouse, PVH neurons are generated between embryonic day 10.5 (E10.5) and E12.5, and their terminal differentiation completes largely before birth (*4*–*6*). Mutant studies in mice have illustrated that the specification of PVH neurons is programmed by a cascade of transcription factors (TFs) including single-minded 1 (SIM1), which is highly expressed in the anterior hypothalamus during embryogenesis and persists in most PVH neurons of adult brain (*5*, *7*, *8*). Using SIM1 as a specific marker of PVH neurons, the functions of various neuronal subtypes including peptidergic neurons such as vasopressin (AVP$^+$), oxytocin (OXT$^+$), corticotropin-releasing hormone (CRH$^+$), thyrotropin-releasing hormone (TRH$^+$), and prodynorphin (PDYN$^+$) neurons, as well as nonpeptidergic neurons such as melanocortin-4 receptor (MC4R$^+$) and nitric oxide synthase–1 (NOS1$^+$) neurons, have been examined in appetite regulation (*3*, *9*–*12*). However, although SIM1$^+$ PVH neurons have been characterized and are known to be heterogeneous, their molecular identities remain poorly understood at the single-cell level.

In humans, loss-of-function mutations in *SIM1* have been implicated in hyperphagic childhood obesity (*13*–*16*). Knockout (KO) of *Sim1* in mice (*Sim1*$^{-/-}$, *Sim1*^{KO}) results in perinatal lethality and the absence of multiple neuroendocrine cell types in the PVH, unveiling a pivotal role for SIM1 in the formation of PVH neurons (*5*). Similar to humans, early onset of hyperphagic obesity was found in mice with heterozygous loss of *Sim1* (*17*, *18*). *Sim1*^{Het} (*Sim1*$^{+/-}$) mice exhibit a major reduction of AVP$^+$ and OXT$^+$ neurons, but not CRH$^+$ neurons, in the PVH and compromised melanocortin signaling (*19*–*21*), suggesting that *Sim1* haploinsufficiency results in specific neurodevelopmental defects in the PVH leading to the hyperphagia phenotype. Furthermore, postnatal knockdown or KO of *Sim1* in the PVH neurons of adult mice also resulted in hyperphagia, indicating that *Sim1* function is required in mature PVH neurons for appetite regulation (*22*–*24*).

The *Iroquois* homeobox genes *IRX3* and *IRX5* have been implicated as determinants of human obesity in connection with the intronic variants of *FTO* (*25*–*27*). We have recently demonstrated that *Irx3* and *Irx5* are expressed in multiple cell types of the mouse hypothalamic arcuate-median eminence (ARC-ME), and their activities regulate hypothalamic leptin sensitivity and food intake (*28*). *Irx3* was previously shown to be ectopically expressed in the anterior hypothalamus of E12.5 *Sim1*^{KO} embryos (*7*), suggesting that this misexpression has the potential to disrupt the formation of PVH neurons in *Sim1*^{KO} mice. Thus, we are intrigued to investigate whether ectopic misexpression of *Irx3* and *Irx5* is also found in the anterior hypothalamus of *Sim1*^{Het} mice, and whether they contribute to the neurodevelopmental defects of the PVH underlying the hyperphagia phenotype of *Sim1* haploinsufficiency.

In this study, we used the *Sim1-Cre*;Ai14 *tdTomato* labeling system (*12*, *29*) to track the *Sim1*$^+$ cell lineage along with single-cell RNA sequencing (scRNA-seq) analysis to explore the cellular and molecular profiles of the PVH neurons and identified two major populations of *Sim1-Cre*$^+$ PVH neurons, which are differentially affected by *Sim1* haploinsufficiency. We demonstrated that *Irx3* and *Irx5* are ectopically expressed in the *Sim1-Cre*$^+$ PVH cells of *Sim1*^{Het} mice. Through reduction of *Irx3* or/and *Irx5* dosage as well as conditional KO of *Irx3* in *Sim1-Cre*$^+$ PVH cells, our analysis demonstrates that the abnormal expression of *Irx3* and *Irx5* leads to the neurodevelopmental defects and hyperphagia in *Sim1* haploinsufficiency.

[1]Program in Developmental and Stem Cell Biology, The Hospital for Sick Children, Toronto, ON M5G 0A4, Canada. [2]Department of Molecular Genetics, University of Toronto, Toronto, ON M5S 1A8, Canada. [3]Department of Neurosurgery, Xiangya Hospital, Central South University, Changsha, Hunan 410008, China. [4]Hunan International Scientific and Technological Cooperation Base of Brain Tumor Research, Xiangya Hospital, Central South University, Changsha, Hunan 410008, China. [5]CHU Sainte-Justine Research Center, Montreal, QC H3T 1C5, Canada. [6]Departments of Pediatrics and Neurosciences, Université de Montréal, Montreal, QC H3T 1J4, Canada.
*Corresponding author. Email: joeeun.son@sickkids.ca (J.E.S.); cchui@sickkids.ca (C.-c.H.)
†Present address: University of Ottawa Heart Institute and Department of Cellular and Molecular Medicine, University of Ottawa, Ottawa, ON, Canada.

These observations establish a novel disease mechanism underlying the hyperphagic obesity of *Sim1* haploinsufficiency and illustrate that *Irx3* and *Irx5* are also involved in obesity due to defective feeding regulation.

RESULTS

scRNA-seq analysis reveals two major PVH neuronal populations

To define the cellular and molecular profiles of PVH neurons, as well as the effects of *Sim1* haploinsufficiency on PVH neurons, we performed scRNA-seq analysis of *Sim1-Cre*$^{+}$ hypothalamic cells from control and *Sim1*^{Het} neonatal mice. We used *Sim1-Cre* (*12*) and the Ai14 *tdTomato* reporter system (*29*) to mark PVH cells at postnatal day 1 (P1) to P4, when differentiation of PVH neurons is complete. Through fluorescence-activated cell sorting, we isolated tdTomato^{+} (*Sim1-Cre*$^{+}$) cells from hypothalami excluding the supraoptic nucleus, which also contains *Sim1*$^{+}$ cells, and prepared single-cell libraries for transcriptome analysis (Fig. 1A).

Through graph-based clustering, we projected 5283 individual cells (2807 from control and 2476 from *Sim1*^{Het}) onto a uniform manifold approximation and projection (UMAP) plot, yielding three distinct cell clusters (Fig. 1B). Using the expression patterns of previously established marker genes and differentially expressed genes found in each cell cluster, we identified a progenitor population enriched in *Sox2* expression and two neuronal populations ("neuron 1" and "neuron 2"), both with high expression of pan-neuronal markers *Elavl3* and *Tubb3* (Fig. 1, B to D, and fig. S1). Neuron 1 is enriched in the expression of genes encoding TFs including *Foxb1*, *Lhx1*, and *Pou2f2*, as well as the *Cck*, *Cartpt*, and *Nts* neuropeptides, whereas neuron 2 shows high gene expression of TFs, including *Otp*, *Nr2f2* (*COUP-TFII*), *Pou3f2* (*Brn2*), and *Onecut2*, and neuropeptides/enzymes, including *Avp*, *Oxt*, *Pdyn*, *Trh*, *Crh*, *Nos1*, and *Mc4r* (Fig. 1D and fig. S1). Immunostaining of markers for the two neuronal populations [Cocaine- and amphetamine-regulated transcript (CART) for neuron 1 and AVP, NOS1, and OXT for neuron 2] confirms the presence of these neuronal subtypes in the PVH (Fig. 1G and fig. S3C). It is important to note that Orthopedia (OTP) and POU domain, class 3, transcription factor 2 (POU3F2), which are highly expressed in neuron 2, are known to act in concert with SIM1 in the terminal differentiation of specific PVH neurons, e.g., AVP^{+} and OXT^{+} neurons (*5*, *6*, *8*, *30*–*32*). Neuron 2 contains many known players in feeding regulation including AVP^{+}, NOS1^{+}, OXT^{+}, PDYN^{+}, and MC4R^{+} neurons (*3*, *9*–*11*). In contrast, the functional role of neuron 1 cells in the control of energy homeostasis is not well understood. These results unveil the presence of two major molecularly distinct *Sim1-Cre*$^{+}$ neuronal populations in the PVH, further illustrating the heterogeneity of PVH neurons.

Sim1 haploinsufficiency disrupts formation of specific PVH neurons

Sim1^{Het} mice display a reduction in PVH cell density, area, and number of nuclear profiles (*5*, *18*). However, analysis of *Sim1*^{Het} mice using a Sim1–green fluorescent protein (GFP) reporter did not reveal a significant difference in the number and area of GFP-positive neurons in the PVH (*21*). By *Sim1-Cre*;Ai14 *tdTomato* labeling of the PVH, we also did not observe any difference between control and *Sim1*^{Het} mice in the number of tdTomato^{+} cells or the proportion of neurons as marked by HuC (fig. S2, A to C). Consistent with this, similar proportions of neurons were detected in the *Sim1-Cre*$^{+}$ scRNA-seq datasets of control and *Sim1*^{Het} mice (fig. S2, D to F). Despite the observation that overt neuronal differentiation is not affected by *Sim1* haploinsufficiency, we observed a marked difference in the composition of neuronal populations in *Sim1*^{Het} mice. When compared with the control, there is a significant increase of the neuron 1 population accompanied by a reduction of the neuron 2 population (Fig. 1E). The proportion of cells expressing markers enriched in neuron 1 was higher in *Sim1*^{Het} mice, whereas that of cells expressing markers enriched in neuron 2 was lower in *Sim1*^{Het} mice (Fig. 1F and fig. S3, A and B). Specifically, formation of some neuron 2 cell types including AVP^{+} and OXT^{+} neurons, as well as NOS1^{+} neurons, is negatively affected by *Sim1* haploinsufficiency, whereas other neuron 2 cell types such as CRH^{+} and TRH^{+} neurons are not as sensitive to *Sim1* gene dosage. Our data unveiled that a subset of PVH neurons (neuron 1) is augmented by *Sim1* haploinsufficiency. Consistent with previous results (*19*, *20*), we showed by immunostaining that there is a marked reduction in the number of AVP^{+} and OXT^{+} PVH neurons (neuron 2) in both P0 and adult *Sim1*^{Het} mice (Fig. 1, G and H, and fig. S3, C and D). In addition, we demonstrated a reduced number of NOS1^{+} neurons (neuron 2) and an increased number of CART^{+} neurons (neuron 1) in the PVH of *Sim1*^{Het} mice. This analysis indicates that *Sim1* haploinsufficiency affects the formation of a specific subset of PVH neurons.

Irx3 and *Irx5* are ectopically expressed in *Sim1-Cre*$^{+}$ PVH cells of *Sim1*^{Het} mice

In E11.5 *Sim1*^{KO} mouse embryos (*7*), *Irx3* was found to be ectopically expressed in the anterior hypothalamus, which gives rise to the PVH. To investigate whether *Sim1*^{Het} mice show ectopic expression of *Irx3* and *Irx5*, we performed RNA in situ hybridization and quantitative polymerase chain reaction (qPCR) analyses. Intriguingly, we found that *Irx3* and *Irx5* are both misexpressed in the anterior hypothalamus of E11.5 *Sim1*^{Het} embryos, and their ectopic expression persists in the PVH of *Sim1*^{Het} mice at P0 (Fig. 2, A and B). In contrast, we did not detect any abnormal expression of *Irx3* and *Irx5* in the hypothalamic ARC-ME of *Sim1*^{Het} mice (Fig. 2, A and C). By costaining *tdTomato* and *Irx3* or *Irx5* RNA, we confirmed that *Irx3* and *Irx5* are misexpressed in *Sim1-Cre*$^{+}$ PVH cells of *Sim1*^{Het} mice (Fig. 2D). This was further supported by qPCR analysis of tdTomato-positive cells sorted from the hypothalamus of *Sim1-Cre*;Ai14 *tdTomato* mice (Fig. 2E). However, we were unable to detect ectopic expression of *Irx3* and *Irx5* in the *Sim1-Cre*$^{+}$ cells from *Sim1*^{Het} mice by scRNA-seq analysis. We postulate that this is due to the limited sequencing depth of the droplet-based scRNA-seq pipeline (*33*, *34*). Together, our results illustrate the ectopic expression of *Irx3* and *Irx5* in the *Sim1-Cre*$^{+}$ PVH cells of *Sim1*^{Het} mice.

A half-reduction of *Irx3* or *Irx5* dosage in *Sim1*^{Het} mice suppresses hyperphagic obesity

To test whether abnormal expression of *Irx3* and *Irx5* in the PVH of *Sim1*^{Het} mice contributes to the hyperphagic obesity phenotype, we generated *Sim1*^{Het} mouse lines lacking one copy of *Irx3* (*Sim1*^{Het};*Irx3*^{Het}) or *Irx5* (*Sim1*^{Het};*Irx5*^{Het}) and confirmed that expression levels of *Irx3* or *Irx5* in *Sim1-Cre*$^{+}$ PVH cells are reduced by ~50% after deleting one allele of *Irx3* or *Irx5*, respectively, without affecting *Sim1* expression in these mutants (figs. S4A and S5A). We further examined the effects of a half-reduction of *Irx3* or *Irx5* dosage on hyperphagia and other metabolic phenotypes. While

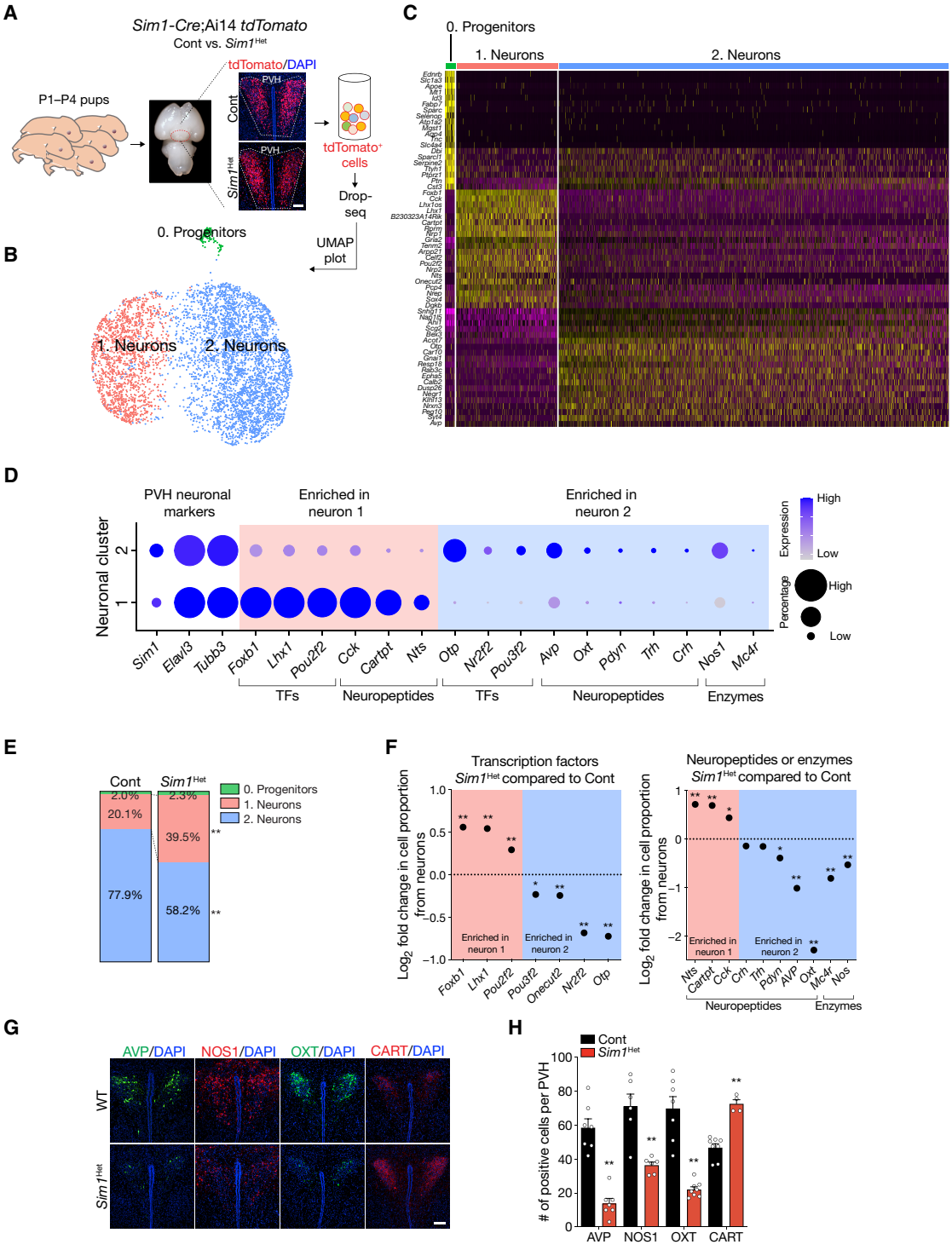

Fig. 1. scRNA-seq analysis of *Sim1-Cre*$^+$ cells reveal characteristics of PVH neurons and their disruption in *Sim1* haploinsufficiency. (**A**) Schematic illustration of live (Sytox blue$^-$) tdTomato$^+$ cells prepared from hypothalami of P1-P4 *Sim1-Cre*;Ai14 *tdTomato* mice for scRNA-seq analysis. DAPI, 4′,6-diamidino-2-phenylindole. (**B**) UMAP plot of sequenced tdTomato$^+$ cells annotated according to known cell type markers. (**C**) Heatmap of top marker genes for each cell cluster and annotation. (**D**) Dot plot showing the expression levels (color) and percentages (size) of cells expressing TFs and neuropeptides/enzymes enriched in each cluster. (**E**) Proportional distribution of cell types as revealed by scRNA-seq analysis. (**F**) Cell type proportional changes in *Sim1*^{Het} versus control samples based on marker gene expression. (**G**) Representative images and (**H**) quantification of the number of AVP$^+$ cells, NOS1$^+$ cells, OXT$^+$ cells, and CART$^+$ cells in the PVH of P0 mice ($n = 7/7$ for AVP$^+$; $n = 6/6$ for NOS1$^+$; $n = 7/7$ for OXT$^+$; $n = 8/5$ for CART$^+$). Data are represented as means ± SEM values. *$P < 0.05$; **$P < 0.01$. WT, wild type. Scale bars, 100 μm.

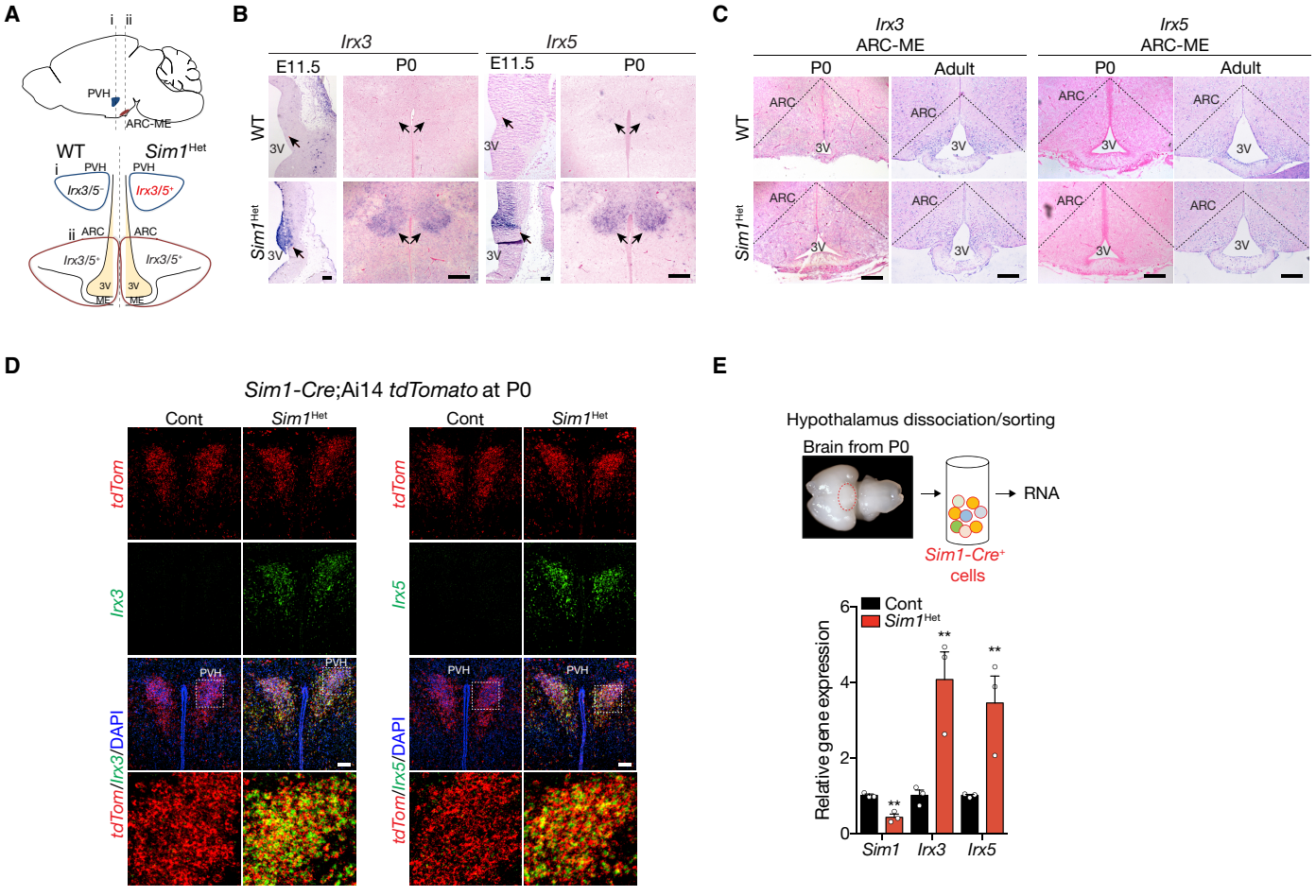

Fig. 2. Ectopic expression of *Irx3* and *Irx5* in the *Sim1-Cre*$^{+}$ PVH cells of *Sim1*^{Het} mice. (**A**) Histological maps illustrating the expression pattern of *Irx3* and *Irx5* in the WT and *Sim1*^{Het} hypothalamus. Section (i) for the PVH and section (ii) for the ARC-ME. 3V, third ventricle. (**B**) In situ hybridization of *Irx3* and *Irx5* mRNA in the anterior hypothalamus (black arrows) of E11.5 embryos and PVH (black arrows) of P0 mice. (**C**) In situ hybridization of *Irx3* and *Irx5* mRNA in the ARC-ME (dashed lines) of P0 and adult mice. (**D**) Fluorescence in situ hybridization of *Irx3*, *Irx5*, and *tdTomato* RNA in the PVH of P0 *Sim1-Cre;*Ai14 *tdTomato* and *Sim1-Cre;*Ai14 *tdTomato;Sim1*^{Het} mice. (**E**) Top: Isolation of *Sim1-Cre*$^{+}$ cells from P0 hypothalami using the *Sim1-Cre*;Ai14 *tdTomato* system. Bottom: Gene expression analysis in *Sim1-Cre*$^{+}$ cells from control and *Sim1*^{Het} mice (Cont/*Sim1*^{Het}: $n = 3/3$). Data are represented as means ± SEM values. $^{**}P < 0.01$. Scale bars, 100 μm.

Irx3^{Het} and *Irx5*^{Het} mice appeared wild type and did not show any obvious body weight and mass phenotypes (*28*), both *Sim1*^{Het};*Irx3*^{Het} and *Sim1*^{Het};*Irx5*^{Het} mice exhibited a less obese phenotype including a clear reduction of body weight, adiposity, and other metabolic abnormalities (i.e., hepatosteatosis and glucose intolerance) compared to *Sim1*^{Het} mice (Fig. 3, A to F, and I to N). Notably, reduction of *Irx3* or *Irx5* dosage significantly suppressed excessive food intake without affecting energy expenditure, respiratory exchange ratio (RER), and locomotor activity (Fig. 3, G, H, and O to P, and figs. S4, B to F, and S5, B to F). These results support the notion that misexpression of *Irx3* and *Irx5* in *Sim1*^{Het} mice is involved in the hyperphagia phenotype.

A simultaneous reduction of *Irx3* and *Irx5* completely overrides obesity in *Sim1*^{Het} mice

Because a half-reduction of *Irx3* or *Irx5* dosage partially suppressed the phenotype of *Sim1*^{Het} mice, we investigated whether simultaneous reduction of *Irx3* and *Irx5* can further ameliorate the hyperphagic obesity due to *Sim1* haploinsufficiency. By using mice harboring the *cis*-heterozygous mutant alleles of *Irx3* and *Irx5* (*Irx3/5*^{dHet}), we generated *Sim1*^{Het};*Irx3/5*^{dHet} mice and confirmed a half-reduction of *Irx3* and *Irx5* expression, but not *Sim1*, in *Sim1-Cre*$^{+}$ PVH cells of *Sim1*^{Het};*Irx3/5*^{dHet} mice compared to *Sim1*^{Het} mice (fig. S6A). In our recent study (*28*), simultaneous reduction of *Irx3* and *Irx5* dosage in mice (*Irx3/5*^{dHet}) was shown to result in a lean phenotype through increased energy expenditure due to adipose browning and elevated leptin sensitivity with reduced food intake. Notably, *Sim1*^{Het};*Irx3/5*^{dHet} mice exhibited a lean phenotype almost identical to that of *Irx3/5*^{dHet} mice (Fig. 4, A and B). Both *Sim1*^{Het};*Irx3/5*^{dHet} and *Irx3/5*^{dHet} mice were leaner than wild-type mice and showed reduced adiposity (Fig. 4, C to E). Furthermore, major metabolic complications of obesity such as hepatosteatosis and glucose intolerance in *Sim1*^{Het} mice were completely rescued by the simultaneous reduction of *Irx3* and *Irx5* dosage (Fig. 4, E and F). Similar to *Irx3/5*^{dHet} mice, *Sim1*^{Het};*Irx3/5*^{dHet} mice also showed increased energy expenditure and lower food intake (Fig. 4, G and H, and fig. S6B) but without observable differences in RER and locomotor activity (fig. S6, C to F). These results reveal that the haploinsufficiency effects of *Sim1* on food intake regulation

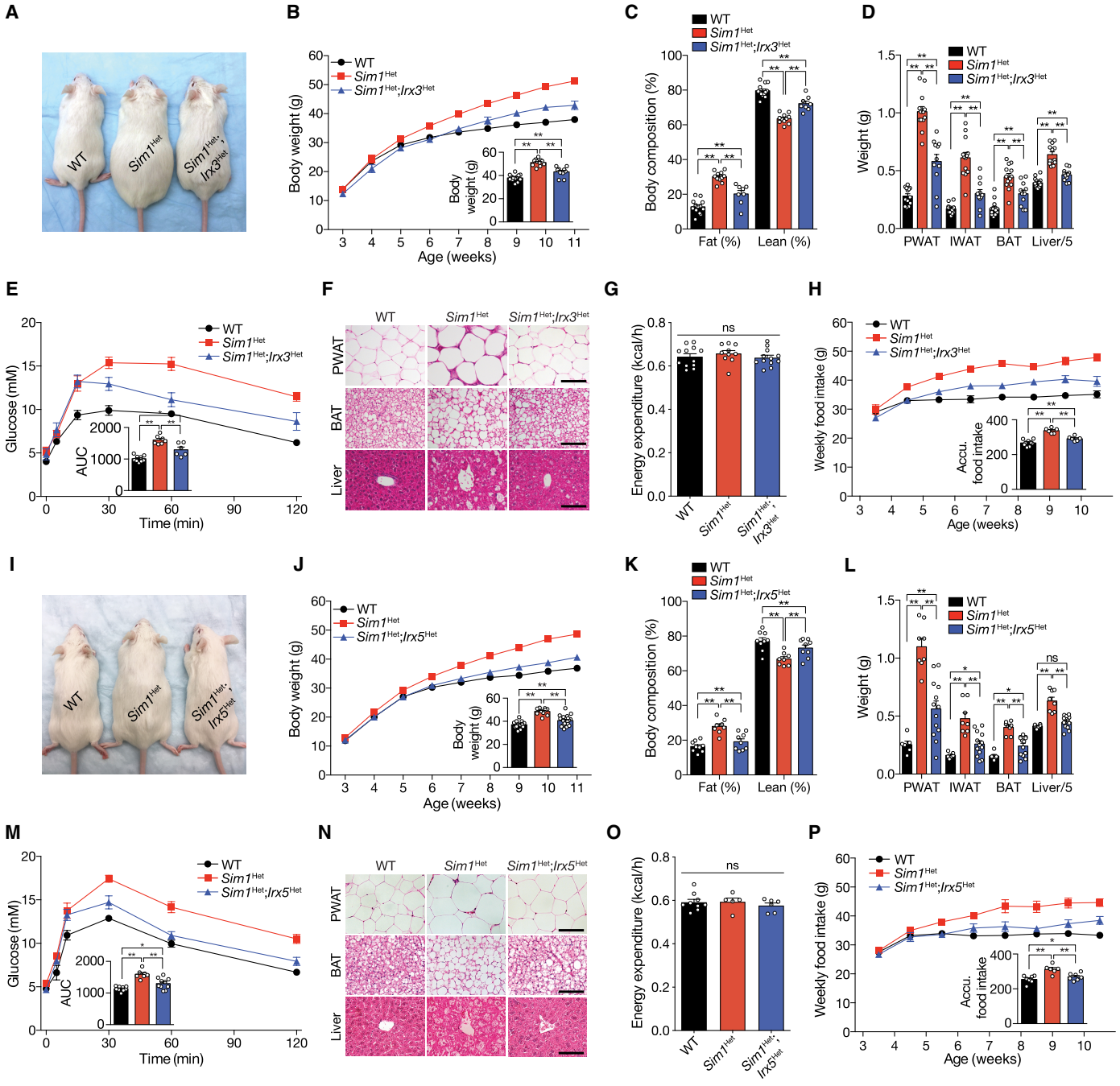

Fig. 3. Reduced dosage of *Irx3* or *Irx5* in *Sim1*^{Het} mice partially suppresses hyperphagic obesity. (**A**) Gross appearance of WT, *Sim1*^{Het}, and *Sim1*^{Het};*Irx3*^{Het} mice at 11 weeks old. Photo credit: Joe Eun Son, The Hospital for Sick Children. (**B**) Body weight and the inset bar graph show body weight of 11-week-old mice (WT, *Sim1*^{Het}, and *Sim1*^{Het};*Irx3*^{Het}; n = 13/11/10). (**C**) Body composition analysis of 12-week-old mice (n = 13/11/8). (**D**) Tissue weight of perigonadal white adipose tissue (PWAT), inguinal WAT (IWAT), brown adipose tissue (BAT), and liver (n = 13/13/11). (**E**) Glucose tolerance tests (GTTs). The inset bar graph shows area under curve (AUC). n = 9/7/6. (**F**) Hematoxylin and eosin (H&E) staining of PWAT, BAT, and liver sections. (**G**) Daily energy expenditure adjusted with lean mass of 29.0 g using analysis of covariance (ANCOVA) of WT, *Sim1*^{Het}, and *Sim1*^{Het};*Irx3*^{Het} mice (n = 12/10/12). (**H**) Food intake. The inset bar graph shows total food intake until 11 weeks of age (n = 9/6/6). (**I**) Gross appearance of WT, *Sim1*^{Het}, and *Sim1*^{Het};*Irx5*^{Het} mice at 11 weeks old. Photo credit: Joe Eun Son, The Hospital for Sick Children. (**J**) Body weight. The inset bar graph shows body weight of 11-week-old mice (WT, *Sim1*^{Het}, and *Sim1*^{Het};*Irx5*^{Het}; n = 15/11/21). (**K**) Body composition analysis at 12 weeks of age (n = 9/8/9). (**L**) Tissue weight of PWAT, IWAT, BAT, and liver (n = 6/8/13). (**M**) GTTs. The inset bar graph shows AUC. n = 9/7/10. (**N**) H&E staining of PWAT, BAT, and liver sections. (**O**) Daily energy expenditure adjusted with a lean mass of 29.6 g using ANCOVA of WT, *Sim1*^{Het}, and *Sim1*^{Het};*Irx5*^{Het} mice (n = 9/5/6). (**P**) Food intake. The inset bar graph shows total food intake until 11 weeks of age (n = 7/6/7). Data are represented as means ± SEM values. *P < 0.05; **P < 0.01, ns, not significant. Scale bars, 100 μm.

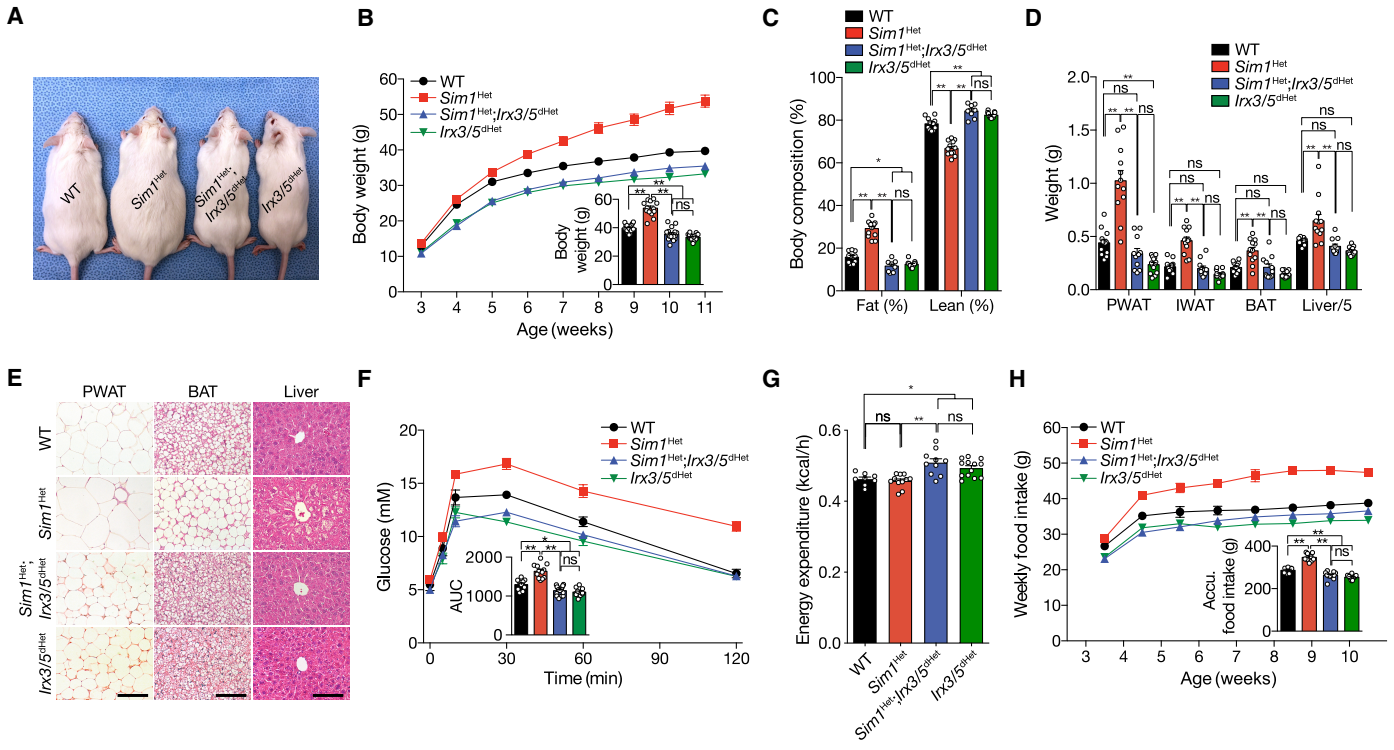

Fig. 4. A simultaneous reduction of *Irx3* and *Irx5* in *Sim1*^{Het} mice overrides hyperphagia. (**A**) Gross appearance of 11-week-old mice. Photo credit: Joe Eun Son, The Hospital for Sick Children. (**B**) Body weight of WT, *Sim1*^{Het}, *Sim1*^{Het};*Irx3/5*^{dHet}, and *Irx3/5*^{dHet} mice. The inset bar graph shows body weight of 11-week-old mice (n = 18/13/17/21). (**C**) Body composition analysis of WT, *Sim1*^{Het}, *Sim1*^{Het};*Irx3/5*^{dHet}, and *Irx3/5*^{dHet} mice at 12 weeks of age (n = 11/13/8/13). (**D**) Tissue weight of PWAT, IWAT, BAT, and liver (n = 13/12/11/14). (**E**) H&E staining of PWAT, BAT, and liver sections. (**F**) GTTs. The inset bar graph shows AUC (n = 10/12/17/11). (**G**) Daily energy expenditure adjusted with a lean mass of 26.1 g using ANCOVA (n = 10/11/10/9). (**H**) Food intake. The inset bar graph shows total food intake until 11 weeks of age (n = 8/10/12/14). Data are represented as means ± SEM values. *P < 0.05; **P < 0.01. Scale bars, 100 μm.

and obesity can be completely overridden in mice by a simultaneous half-reduction of *Irx3* and *Irx5* dosage, pinpointing the central roles of *Irx3* and *Irx5* activities underlying the hyperphagic obesity of *Sim1*^{Het} mice.

Reduction of *Irx3* and *Irx5* restores formation of PVH neurons in *Sim1*^{Het} mice

Next, we sought to determine whether reduction of *Irx3* and *Irx5* in *Sim1*^{Het} mice can restore the PVH neuronal populations to suppress hyperphagia. Notably, we found that simultaneous reduction of *Irx3* and *Irx5* dosage significantly restores PVH neuronal populations in *Sim1*^{Het} mice. The number of AVP^{+}, NOS1^{+}, and OXT^{+} PVH neurons (neuron 1) was significantly restored in *Sim1*^{Het};*Irx3/5*^{dHet} mice compared to *Sim1*^{Het} mice (Fig. 5, A and B). Furthermore, the number of CART^{+} PVH neurons (neuron 2) was also significantly reduced in *Sim1*^{Het};*Irx3/5*^{dHet} mice to a level closer to wild-type mice. Consistent with this, activation of these PVH neurons by the melanocortin agonist melanotan-2 (MTII), as revealed by staining of c-Fos^{+} cells (Fig. 5, C and D), was markedly enhanced in *Sim1*^{Het};*Irx3/5*^{dHet} mice compared with *Sim1*^{Het} mice, suggesting that melanocortin signaling is restored by reduction of *Irx3* and *Irx5* in the PVH of *Sim1*^{Het} mice. While these phenotypes are only partially rescued when compared with wild-type controls and *Irx3/5*^{dHet} mice, these results indicate that misexpression of *Irx3* and *Irx5* indeed contributes to the neurodevelopmental defects of *Sim1*^{Het} mice.

PVH deletion of *Irx3* in *Sim1*^{Het} mice restores the hyperphagic obesity phenotype and neuronal disruption

Next, to specifically examine the effects of ectopic *Irx3* expression in the *Sim1-Cre*$^{+}$ PVH cells on the hyperphagic and neurodevelopmental phenotype in *Sim1*^{Het} mice, we generated mice with deletion of *Irx3* in the *Sim1*$^{+}$ lineage using an *Irx3*-floxed allele (*Irx3*^{Fl}) (*35*) and the *Sim1-Cre* mouse line (*12*) (Fig. 6A). *Sim1-Cre*;*Irx3*$^{Fl/Fl}$ (hereafter PVH-*Irx3*^{KO}) mice did not exhibit any observable differences in body weight, adiposity, and PVH neuronal populations (fig. S7), consistent with the lack of *Irx3* and *Irx5* expression in normal PVH (Fig. 2, A and B). These results suggest that *Irx3*, and likely *Irx5*, is dispensable in the normal PVH. On the other hand, when *Irx3* is specifically deleted in the *Sim1-Cre*$^{+}$ PVH cells of *Sim1*^{Het} mice (*Sim1*^{Het};*Sim1-Cre*;*Irx3*$^{Fl/+}$ and *Sim1*^{Het};*Sim1-Cre*;*Irx3*$^{Fl/Fl}$, hereafter *Sim1*^{Het};PVH-*Irx3*^{Het} and *Sim1*^{Het};PVH-*Irx3*^{KO}, respectively) (Fig. 6A and fig. S8A), the body weight and adiposity of *Sim1*^{Het} mice were markedly reduced in an *Irx3* dosage-dependent manner (Fig. 6, B to D and F). Further analysis of *Sim1*^{Het};PVH-*Irx3*^{KO} mice revealed that obesity-driven metabolic abnormalities such as glucose intolerance and hepatosteatosis are markedly suppressed by *Sim1-Cre* mediated deletion of *Irx3* in *Sim1*^{Het} mice (Fig. 6, E and F). Furthermore, *Sim1*^{Het};PVH-*Irx3*^{KO} mice exhibited no significant differences in energy expenditure, RER, and locomotor activity when compared with control and *Sim1*^{Het} mice (Fig. 6G and fig. S8, B to F) but showed a major reduction in food intake (Fig. 6H), indicating that the reduced body weight of these mice is

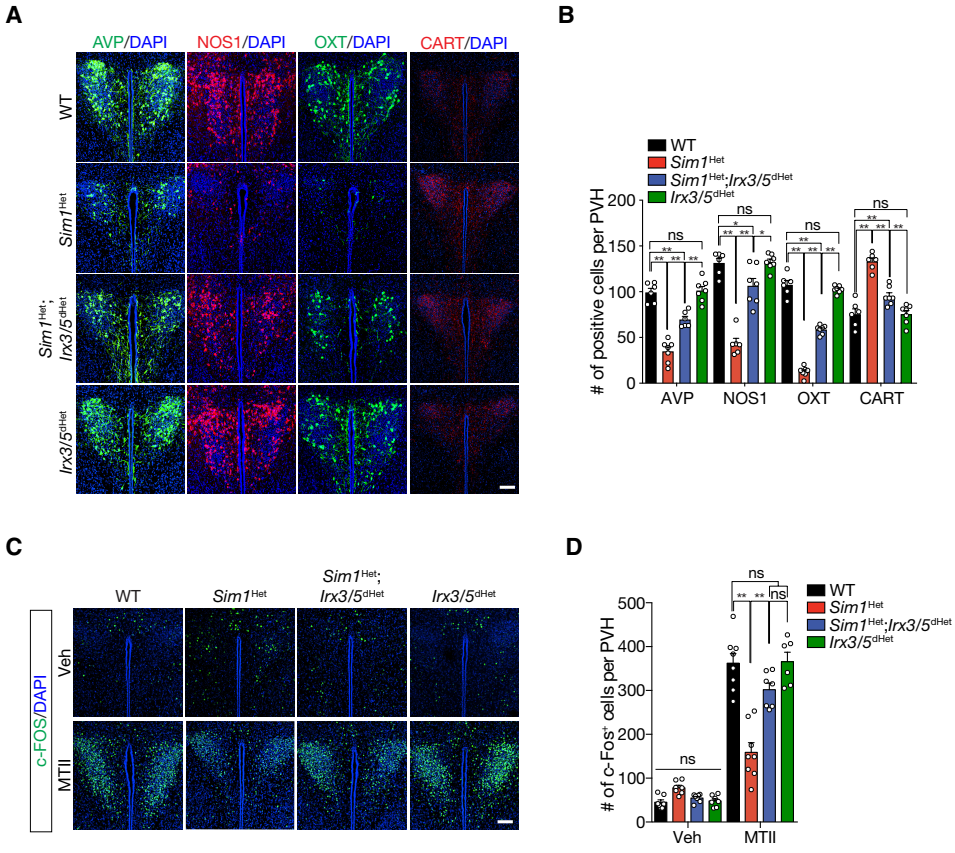

Fig. 5. Reduction of *Irx3* and *Irx5* in *Sim1*^{Het} mice restores the PVH neuronal population. (**A**) Representative images and (**B**) quantification of the number of AVP$^+$ cells, NOS1$^+$ cells, OXT$^+$ cells, and CART$^+$ cells in the PVH ($n = 6/7/6/7$ for AVP$^+$; $n = 6/6/7/7$ for NOS1$^+$; $n = 6/7/7/10$ for OXT$^+$; $n = 6/6/7/7$ for CART$^+$). (**C**) Representative images and (**D**) quantification of the number of c-Fos$^+$ cells in the PVH following MTII injection (vehicle: $n = 7/7/7/7$; MTII: $n = 8/8/7/6$). Data are represented as means ± SEM values. $^*P < 0.05$; $^{**}P < 0.01$. Scale bars, 100 μm.

due to the suppression of the hyperphagia phenotype of *Sim1* haploinsufficiency. Similar to those observed in *Sim1*^{Het};*Irx3/5*^{dHet} mice, the number of AVP$^+$, NOS1$^+$, and OXT$^+$ PVH neurons as well as CART$^+$ PVH neurons were largely restored to a control level in *Sim1*^{Het};PVH-*Irx3*^{KO} mice (Fig. 6, I and J). As revealed by staining of c-Fos$^+$ cells, activation of PVH neurons by the melanocortin agonist MTII was clearly elevated in *Sim1*^{Het};PVH-*Irx3*^{KO} compared to *Sim1*^{Het} mice (Fig. 6, K and L). These observations indicate that deletion of *Irx3* in the PVH of *Sim1*^{Het} mice could significantly restore the PVH neuronal population and their response to melanocortin. It is noteworthy that *Sim1*^{Het};PVH-*Irx3*^{KO} mice still exhibit mild hyperphagic obesity and PVH neuronal disruption phenotypes compared to control mice (Fig. 6), which may be due to remaining *Irx5* misexpression in the PVH of these mice (fig. S8A). Together, our data support the notion that misexpression of *Irx3* and likely *Irx5* in the *Sim1-Cre*$^+$ PVH cells is largely responsible for the neurodevelopmental and hyperphagic obesity phenotypes of *Sim1*^{Het} mice.

DISCUSSION

In this study, we uncovered ectopic PVH expression of *Irx3* and *Irx5* as a novel disease mechanism underlying the hyperphagic obesity of *Sim1* haploinsufficiency in mice (Fig. 7). These results suggest that *IRX3* and *IRX5* are also involved in monogenic obesity disorders of *SIM1* haploinsufficiency (*13*–*15*) besides their implicated roles in *FTO*-associated obesity at the population level (*25*, *26*). It has been established that defective feeding regulation leading to hyperphagia is caused by insufficient *Sim1* activity, as CRISPR-mediated activation of the remaining functional *Sim1* gene in *Sim1*^{Het} mice could rescue the obesity phenotype (*36*). However, the molecular mechanisms underlying *Sim1* haploinsufficiency remain undefined. By using various genetic mouse models, our analysis here provides strong evidence demonstrating that the neurodevelopmental defects in *Sim1*^{Het} mice are at least partly due to ectopic expression of *Irx3* and *Irx5* in the PVH.

Recently, we demonstrated that *Irx3* and *Irx5* play overlapping functions in the control of food intake and energy expenditure (*28*). *Irx3/5*^{dHet} mice exhibit adipose browning resulting in elevated energy expenditure. In addition, these mice show higher hypothalamic leptin sensitivity in the ARC-ME with a lower food intake. Together, these metabolic features lead to an overall whole-body phenotype, which is leaner than wild-type mice. Notably, we found that a half-reduction of *Irx3* and *Irx5* dosage can override the haploinsufficient effects of *Sim1* on hyperphagia, resulting in a lean phenotype in *Sim1*^{Het};*Irx3/5*^{dHet} mice similar to that of *Irx3/5*^{dHet} mice (Fig. 4). In particular, the food intake of *Sim1*^{Het};*Irx3/5*^{dHet} mice was lower than that of wild-type mice (Fig. 4) despite the incomplete rescue of PVH neuronal defects in *Sim1*^{Het};*Irx3/5*^{dHet} mice (Fig. 5). We postulate that besides a restoration of the feeding regulatory neuronal circuitry in the PVH, lower food intake is likely driven by higher

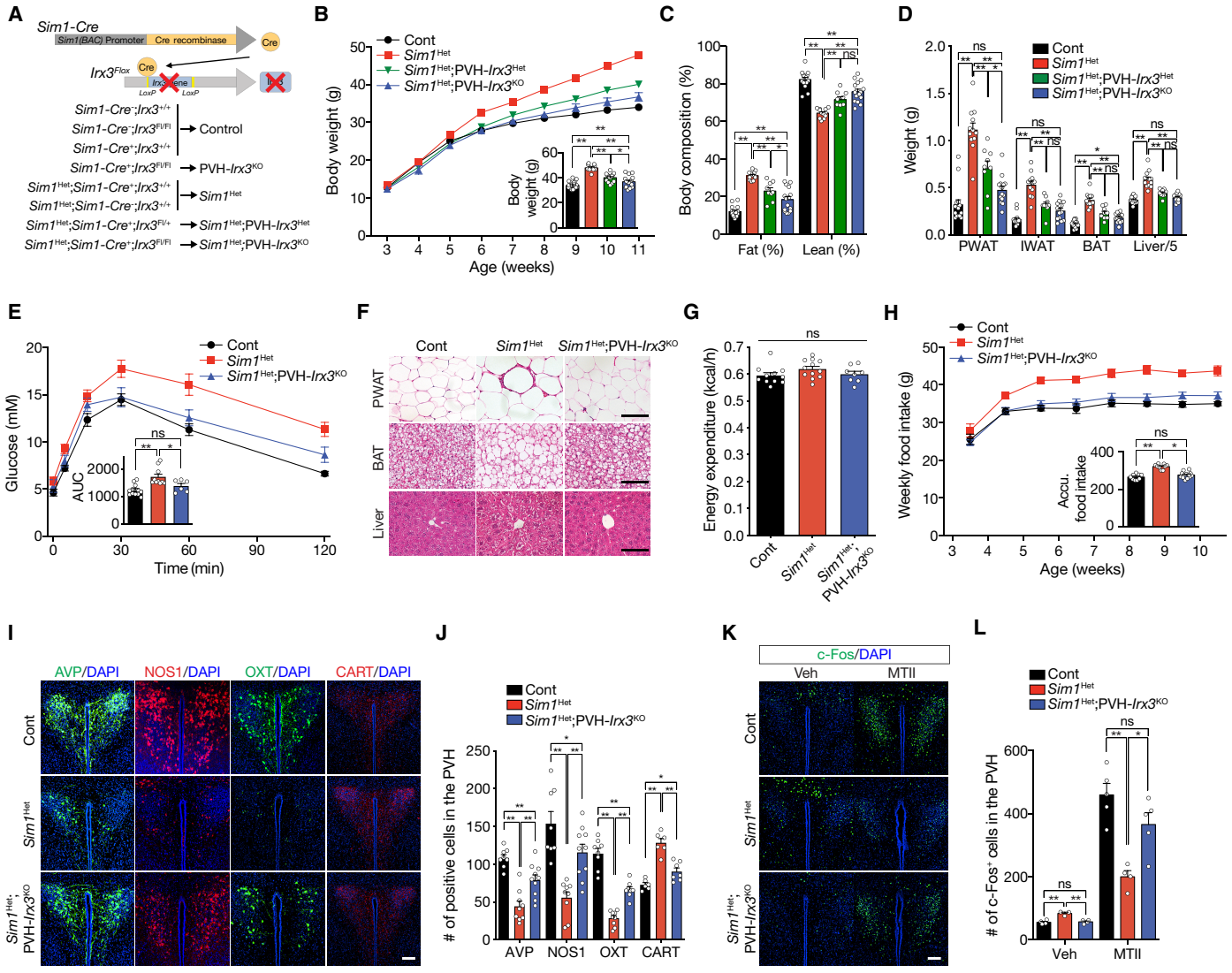

Fig. 6. Deletion of *Irx3* in *Sim1-Cre*$^{+}$ cells of *Sim1*^{Het} mice suppresses hyperphagic obesity and restores PVH neuron formation. (**A**) Breeding scheme for the generation of *Sim1*^{Het};*Sim1-Cre;Irx3*$^{Fl/Fl}$ (*Sim1*^{Het};PVH-*Irx3*^{KO}) mice. (**B**) Body weight of control, *Sim1*^{Het}, *Sim1*^{Het};PVH-*Irx3*^{Het}, and *Sim1*^{Het};PVH-*Irx3*^{KO} mice. The inset bar graph shows body weight of 11-week-old mice ($n = 24/11/15/16$). (**C**) Body composition analysis ($n = 15$ Cont, $n = 12$ *Sim1*^{Het}, $n = 9$ *Sim1*^{Het};PVH-*Irx3*^{Het}, $n = 15$ *Sim1*^{Het};PVH-*Irx3*^{KO}). (**D**) Tissue weight of PWAT, IWAT, BAT, and liver ($n = 15/12/9/14$). (**E**) GTTs. The inset bar graph shows AUC ($n = 13/10/6$). (**F**) H&E staining of PWAT, BAT, and liver sections. (**G**) Daily energy expenditure adjusted with lean mass of 27.6 g using ANCOVA ($n = 11/12/8$). (**H**) Food intake. The inset bar graph shows accumulated food intake until 11 weeks of age ($n = 9/9/13$). (**I**) Representative images and (**J**) quantification of the number of AVP^{+} cells, NOS1^{+} cells, OXT^{+} cells, and CART^{+} cells in the PVH ($n = 8/9/10$ for AVP^{+} or NOS1^{+} or OXT^{+}; $n = 6/7/8$ for CART^{+}). (**K**) Representative images and (**L**) quantification of the number of c-Fos^{+} cells in the PVH following MTII injection (vehicle: $n = 4/3/4$; MTII: $n = 5/4/5$). Data are represented as means ± SEM values. *$P < 0.05$; **$P < 0.01$. Scale bars, 100 μm.

leptin sensitivity in the hypothalamic ARC-ME region of these mice due to their *Irx3/5*^{dHet} background. Moreover, elevated energy expenditure in the *Irx3/5*^{dHet} background also contributes to the lean phenotype. The unexpected observation that the effects of *Sim1* haploinsufficiency can be completely nullified by a half-reduction of *Irx3* and *Irx5* dosage in mice further illustrates the importance of *IRX3* and *IRX5* in energy homeostasis and human obesity.

Several lines of research have suggested regulatory functions of *Irx* genes in the development of the nervous system. Members of the *Drosophila Irx* gene family are implicated in the development of the peripheral nervous system, and *Xenopus Irx* genes are involved in neurogenesis (*37*–*39*). In mice, *Irx* genes are also expressed during early neurogenesis and implicated in the regulation of *Ascl1* (*Mash1*). In the developing nervous system, *Irx3* and *Irx5* display an overlapping expression pattern with *Ascl1* (*40*). Notably, *Ascl1* is critical for the differentiation and specification of hypothalamic neuroendocrine cells (*41*, *42*), suggesting potential involvement of *Irx3* and *Irx5* in neuronal development and specification. Our recent study has demonstrated that *Irx3* and *Irx5* expression in the radial glia-like neural stem cells regulates postnatal neurogenesis in the hypothalamic ARC (*28*). Here, we show that abnormal expression of *Irx3*

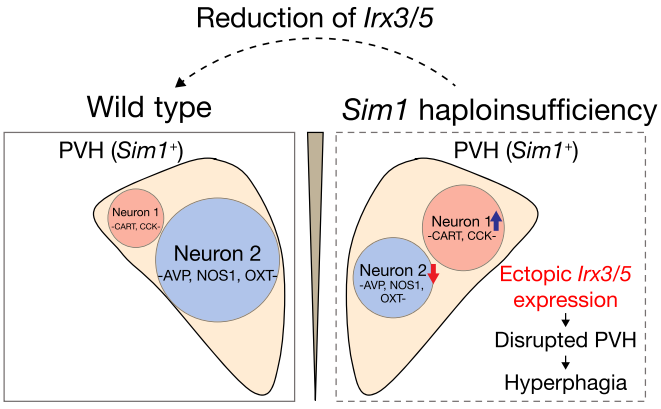

Fig. 7. Model depicting abnormal expression of *Irx3* and *Irx5* in the PVH leads to neurodevelopmental defects and hyperphagic obesity in *Sim1* haploinsufficiency. Two major subpopulations (neuron 1 and neuron 2) of *Sim1-Cre*$^{+}$ PVH neurons are differentially affected by *Sim1* haploinsufficiency. *Irx3* and *Irx5* are ectopically expressed in the *Sim1-Cre*$^{+}$ PVH cells of *Sim1*^{Het} mice and contribute to the PVH neuronal disruption and hyperphagic obesity of *Sim1* haploinsufficiency. Reduction of *Irx3* or/and *Irx5* dosage in *Sim1*^{Het} mice restores the formation of PVH neurons rescuing the hyperphagic obesity phenotype.

and *Irx5* in Sim1^{+} PVH cells in *Sim1* haploinsufficiency contributes to neurodevelopmental defects via disruption of the neuronal populations involved in feeding regulation. Future studies are warranted to investigate the molecular mechanisms underlying *Irx3*- and *Irx5*-mediated PVH neuronal defects in *Sim1* haploinsufficiency. To delineate this question, deletion of both *Irx3* and *Irx5* in *Sim1*$^{+}$ cells would be an ideal experiment. Defining the genes/pathways activated or repressed by *Irx3* and *Irx5* in Sim1^{+} PVH cells should yield deeper insights about neuronal development and specification of PVH.

Many *Sim1*$^{+}$ PVH neuron subtypes have been established for their roles in feeding regulation (*3*, *9*–*12*, *43*). In this study, our lineage tracing and scRNA-seq analyses have revealed additional heterogeneity of *Sim1-Cre*$^{+}$ PVH neurons. Furthermore, we showed that *Sim1* haploinsufficiency affects the formation of specific PVH neurons but not overt neuronal differentiation. On the basis of TF and neuropeptide gene signatures, *Sim1-Cre*$^{+}$ PVH neurons can be clustered into two main groups (Fig. 1D). The neuron 2 population consists of ~80% of *Sim1-Cre*$^{+}$ PVH neurons and is likely quite heterogeneous with enriched expression of OTP, which is known to act in parallel with SIM1 in the specification of PVH neurons including AVP^{+}, OXT^{+}, and CRH^{+} and TRH^{+} neurons (*3*, *6*, *30*, *44*). This group of neurons seems to include most "feeding regulatory" neurons described before. As shown in previous studies (*19*, *20*), our scRNA-seq analysis revealed that AVP^{+} and OXT^{+} neurons are specifically compromised by *Sim1* haploinsufficiency, whereas other neuron 2 subtypes (e.g., CRH^{+} and TRH^{+} neurons) are not as sensitive to the dosage of *Sim1* (Fig. 1F). We detected a drastic reduction of *Otp* expression in the PVH neurons of neonatal *Sim1*^{Het} mice (Fig. 1F and fig. S3A), although *Otp* expression was previously shown to be unaffected by KO of *Sim1* (*6*). Similarly, a significant reduction of *Nr2f2*, which encodes Chicken ovalbumin upstream promoter transcription factor II (COUP-TFII) that is coexpressed with POU3F2 in differentiating PVH neurons (*45*), was also found in these PVH neurons of *Sim1*^{Het} mice, despite the observation that only a slight reduction of *Pou3f2* expression was detected. Thus, our data illustrate that *Sim1* haploinsufficiency could lead to altered expression of *Otp* and *Nr2f2*, contributing to the specific PVH neuronal defects.

In this study, we have identified a poorly characterized population of PVH neurons (neuron 1), which constitutes about 20% of *Sim1-Cre*$^{+}$ PVH neurons and appears to be a homogeneous group with high expression of TFs (*Foxb1*, *Lhx1*, and *Pou2f2*) and little or no expression of *Otp*, *Nr2f2*, and *Pou3f2*. These neurons also express a distinct set of neuropeptides including *Cck*, *Cartpt*, and *Nts*. These neuropeptide-expressing neurons have previously been detected in the PVH (*46*–*48*), but their functions are mostly linked to stress and inflammation. Nonetheless, CART^{+} PVH neurons could be activated by intraperitoneal injection of Cholecystokinin octapeptide (CCK-8S) in rats, suggesting that these neurons may play a role in the anorexigenic effects of peripheral CCK signals (*49*). We found that the number of these PVH neurons is augmented by ~100% in *Sim1*^{Het} mice. Further studies of these PVH neurons in feeding regulation are warranted.

In closing, we illustrated here abnormal hypothalamic activities of *Irx3* and *Irx5* as a central mechanism disrupting the development of PVH neurons leading to defective feeding regulation in *Sim1* haploinsufficiency. However, there are many remaining questions. Additional studies will be needed to decipher how haploinsufficiency of *Sim1* triggers the ectopic PVH expression of *Irx3* and *Irx5* and to determine whether ectopic expression of *Irx3* and/or *Irx5* in the PVH alone is sufficient to induce the neurodevelopmental defects of *Sim1*^{Het} mice. By unveiling the abnormal hypothalamic function of *IRX3* and *IRX5*, our work could also provide potential targets for obesity prevention and treatment.

MATERIALS AND METHODS

Animals

All animal experimental protocols approved by the Animal Care Committee of The Toronto Centre for Phenogenomics conformed to the standards of the Canadian Council on Animal Care. *Sim1*^{Het} mice (*50*), *Irx3*^{tauLacZ} mice (*51*), *Irx5*^{eGFP} mice, *Irx3*$^{-}$*5*^{eGFP} mice, and *Irx3*-floxed (*Irx3*^{Flox}) mice (*35*) were described previously. *Sim1-Cre* (stock no. 006451) and Ai14^{tdTomato} (stock no. 007914) mice were obtained from the Jackson Laboratory. Mice were backcrossed for 10 generations on an outbred CD1 background. To generate *Sim1-Cre*;*Irx3*$^{Fl/Fl}$ mice, *Irx3*$^{Fl/Fl}$ mice were mated with *Sim1-Cre* mice. These mice were bred to *Sim1*^{Het} mice to produce *Sim1*^{Het};*Sim1-Cre*;*Irx3*$^{Fl/Fl}$ mice. The colony was housed in a specific pathogen–free facility in ventilated cages with controlled environment settings (21° to 22°C, 30 to 60% humidity for standard housing), 12-hour light/12-hour dark cycles, and free access to water. Mice were randomly assigned to the experimental groups at the time of weaning.

Flow cytometry analysis and sorting

For *Sim1-Cre*;Ai14 *tdTomato* cell sorting, pups (P0 to P4) were dissected, and then hypothalami were rapidly extracted excluding optic chiasm and supra optic nucleus. Pooled hypothalamus samples from five to six mice were digested by papain solution (Worthington Biochemical) with deoxyribonuclease in Hibernate A medium for 30 min at 37°C with gentle agitation. Digestion was stopped by dilution with Hibernate A containing B27 (Thermo Fisher Scientific), GlutaMAX (Thermo Fisher Scientific), and 5% Trehalose (Sigma-Aldrich) and then gently triturated using a series of three Pasteur pipettes with tips fire-polished to incrementally smaller openings. Cell suspension was centrifuged at

300*g* for 5 min and resuspended in Hanks' balanced salt solution with 0.5% bovine serum albumin (BSA) and 5% Trehalose. Sytox blue (Thermo Fisher Scientific; 1:1000) was added to the cell suspension, and cells were filtered a second time through a 70-μm cell strainer. Viable (Sytox blue–negative) tdTomato$^+$ cells were subsequently sorted using a MoFlo Astrios (Beckman Coulter) cell sorter. Following cell sorting, cells were pelleted at 400*g* for 5 min, resuspended in phosphate-buffered saline (PBS) with 0.01% BSA, and counted with a hemocytometer. Total RNA from *Sim1-Cre*$^+$ marked cells was extracted using the RNeasy Micro Kit (Qiagen).

Single-cell transcriptome sequencing

Following cell sorting, cells were pelleted at 400*g* for 5 min, resuspended in PBS with 0.01% BSA, and counted with a hemocytometer. Cells were adjusted to a final concentration of 140,000 cells/ml. Drop-seq was then carried out at the Princess Margaret Genomics Facility (Toronto, ON) as described previously (*52*), except that flow rates of 3000 (cells and beads) and 13,000 μl/hour (oil) were used, and beads were resuspended at 167,000 per ml. Following Drop-seq droplet collection, complementary DNA amplification and sequencing library preparation were performed as described (*52*), and the libraries were sequenced on a high-output Illumina NextSeq 500 flow cell at the Princess Margaret Genomics Centre (Toronto, ON).

scRNA-seq read alignment

Raw paired-end sequencing reads were processed using the Drop-seq tools (version 1.13) as described previously (*52*). Reads were aligned to the mouse genome (mm10) using STAR v2.6.0b (*53*) with default settings. Following the cell selection method described in the Drop-seq Alignment Cookbook (version 1.2, written by James Nemesh from the McCarroll Lab, http://mccarrolllab.org/dropseq/), the cumulative fractions of reads for each successively smaller cell barcode were plotted to estimate the number of cell barcodes to be extracted from each experimental group. The inflection points of the plots were determined as the number of cell barcodes to be extracted and used in downstream analysis. Digital gene expression (DGE) matrices with 2807 and 2476 cell barcodes were selected for control and *Sim1*^{Het} experimental groups, respectively. To run a single integrated analysis of all cells, DGE matrices were merged together for downstream analysis.

scRNA-seq data analysis

Cell barcodes with at least 200 genes detected were selected for clustering analysis using the Seurat R package (https://satijalab.org/seurat/) (*54*). Briefly, following quality control by mitochondrial gene percentage and removal of cell doublets, gene expression measurements for each cell were divided by total gene expression, multiplied by 10,000, and natural log–transformed. Highly variable genes were identified with default settings of Seurat and used for principal components analysis, following data scaling to remove unwanted sources of variation by regressing on the number of molecules detected per cell and mitochondrial gene percentage. Significant principal components were used as input for UMAP plotting. Cluster markers were identified using the FindAllMarkers function in Seurat. Cluster identities were assigned on the basis of the top highly expressed genes and previously identified the PVH neuronal specific markers (*3*, *9*–*12*, *17*, *19*, *20*, *55*, *56*). All statistical analyses of comparisons between experimental groups were performed using the chi-square test of independence with Bonferroni-adjusted *P* values. A probability value of $P < 0.05$ was used as the criterion for statistical significance.

Metabolic phenotyping experiments

Body weight was measured every week from 3 weeks of age. Body composition was analyzed using an EchoMRI device (Echo Medical Systems). Food intake of individually housed mice was determined as the difference in weight between Food-In and Food-Out, accounting for food spillage onto the cage floor on subsequent weeks, measured weekly from 3 weeks of age. Energy expenditure and RER (RER = VCO_2/VO_2) were evaluated at 8 to 10 weeks of age by indirect calorimetry using the Oxymax Comprehensive Lab Animal Monitoring System (Columbus Instruments) over periods of 24 hours. Briefly, energy expenditure was calculated by multiplying oxygen consumption (VO_2) by the calorific value (calorific value = 3.815 + 1.232 × RER) and analyzed using analysis of covariance (ANCOVA) with lean mass adjustment or lean mass normalization. We simultaneously measured the locomotor activity of each mouse using the break counts of infrared beams. For glucose tolerance tests, mice were subjected to intraperitoneal injection of glucose (1 mg/g of body weight) after fasting overnight (14 to 16 hours). Blood glucose levels were measured at the indicated intervals using a glucometer (Contour NEXT, Bayer HealthCare).

Gene expression analyses by qPCR

Total RNA was extracted from tissue using the Qiagen RNeasy Mini or Micro Kit (Thermo Fisher Scientific), and complementary DNA was synthesized using Moloney-murine leukemia virus (M-MLV) reverse transcriptase (Thermo Fisher Scientific) with oligo(dT). Gene expression assay was conducted using SYBR Green methods on Viia7 (Applied Biosystems), and relative cycle threshold values were normalized by *Actb* (β-actin). The primers used for qPCR are shown in table S1.

In situ hybridization

Tissues were fixed overnight in 4% paraformaldehyde (PFA) at 4°C, processed, embedded in Optimal cutting temperature (OCT) compound, and sectioned at 20-μm thickness using cryostat (Leica) or embedded in paraffin and sectioned at 5-μm thickness using microtome (Leica). Section in situ hybridization against *Irx3*, *Irx5*, and *tdTomato* mRNA was carried out using published procedures with digoxigenin (DIG)–labeled RNA probes and anti–DIG-Peroxidase (POD) antibody (Roche; 1:2000) or fluorescein isothiocyanate–labeled RNA probes and anti–fluorescein isothiocyanate–Peroxidase (POD) antibody (Roche; 1:500) (*40*, *57*, *58*). The probes used for in situ hybridization are shown in table S1.

Histology

Tissues were fixed in 4% PFA and embedded in paraffin. Sections of 5 μm were stained with hematoxylin and eosin. Images were captured using a Nikon Eclipse microscope.

Immunostaining

Mice were deeply anesthetized with isoflurane and transcardially perfused with 1% PFA, and brains were harvested and fixed with 4% PFA. Fixed tissues were washed with PBS, embedded in OCT after cryoprotection with 30% sucrose, and then sectioned at 20-μm thickness using a cryostat (Leica) or 60 μm thickness using a vibratome

(Leica). After antigen retrieval in 10 mM sodium citrate buffer (pH 6.0), brain slices were incubated for 1 hour at room temperature with 0.3% Triton X-100 in PBS (PBST) solution containing 5% donkey serum (Sigma-Aldrich) for blocking and permeabilization. After blocking, the samples were incubated overnight at 4°C with the following primary antibodies: anti-AVP (Millipore, AB1565, Rabbit; 1:5000), anti-NOS1 (Santa Cruz Biotechnology, A-11, Mouse; 1:200), anti-OXT (Millipore, AB911, Rabbit; 1:5000), anti-CART (Pheonix Pharmaceuticals, H-003-62, Rabbit; 1:2000), and anti–c-FOS (Santa Cruz Biotechnology, SC-52, Rabbit; 1:200). After several washes in PBST, tissues were incubated for 2 hours at room temperature with the following secondary antibodies: donkey anti-rabbit Alexa Fluor 488, 555, or 647 (Thermo Fisher Scientific; 1:2000) and donkey anti-mouse Alexa Fluor 488, 555, or 647 (Thermo Fisher Scientific; 1:2000). Slices were counterstained and mounted on the slide with mounting medium (Abcam), and then fluorescence signals were visualized using a Nikon A1R confocal microscope system and analyzed by ImageJ software (National Institutes of Health).

Neuronal activation by melanocortin agonist (MTII)

Six- to 7-week-old mice were fasted for 18 hours, injected with MTII (5 mg/kg; Canada Peptide), and then perfused 2 hours later with 1% PFA. Nuclear c-FOS immunoreactivity was then used as a marker for neuronal activation in PVH subsets.

Statistical analysis

Statistical analyses were performed using PRISM 6.0 software (GraphPad). Data are expressed as the means ± SEM values. Statistical significance of differences among groups was determined by Student's *t* test or one-way analysis of variance (ANOVA) with post hoc analysis. When ANOVA indicated statistical significance, Tukey's honestly significant difference test was then used to determine the significantly different means. A probability value of $P < 0.05$ was used as the criterion for statistical significance.

SUPPLEMENTARY MATERIALS

Supplementary material for this article is available at https://science.org/doi/10.1126/sciadv.abh4503

View/request a protocol for this paper from *Bio-protocol*.

REFERENCES AND NOTES

1. A. P. Coll, I. S. Farooqi, S. O'Rahilly, The hormonal control of food intake. *Cell* **129**, 251–262 (2007).
2. Q. Gao, T. L. Horvath, Neuronal control of energy homeostasis. *FEBS Lett.* **582**, 132–141 (2008).
3. A. K. Sutton, M. G. Myers Jr., D. P. Olson, The role of PVH circuits in leptin action and energy balance. *Annu. Rev. Physiol.* **78**, 207–221 (2016).
4. M. A. Karim, J. C. Sloper, Histogenesis of the supraoptic and paraventricular neurosecretory cells of the mouse hypothalamus. *J. Anat.* **130**, 341–347 (1980).
5. J. L. Michaud, T. Rosenquist, N. R. May, C. M. Fan, Development of neuroendocrine lineages requires the bHLH-PAS transcription factor SIM1. *Genes Dev.* **12**, 3264–3275 (1998).
6. D. Acampora, M. P. Postiglione, V. Avantaggiato, M. di Bonito, F. M. Vaccarino, J. Michaud, A. Simeone, Progressive impairment of developing neuroendocrine cell lineages in the hypothalamus of mice lacking the Orthopedia gene. *Genes Dev.* **13**, 2787–2800 (1999).
7. A. Caqueret, F. Boucher, J. L. Michaud, Laminar organization of the early developing anterior hypothalamus. *Dev. Biol.* **298**, 95–106 (2006).
8. C. Qin, J. Li, K. Tang, The paraventricular nucleus of the hypothalamus: Development, function, and human diseases. *Endocrinology* **159**, 3458–3472 (2018).
9. A. K. Sutton, H. Pei, K. H. Burnett, M. G. Myers, C. J. Rhodes, D. P. Olson, Control of food intake and energy expenditure by Nos1 neurons of the paraventricular hypothalamus. *J. Neurosci.* **34**, 15306–15318 (2014).
10. M. M. Li, J. C. Madara, J. S. Steger, M. J. Krashes, N. Balthasar, J. N. Campbell, J. M. Resch, N. J. Conley, A. S. Garfield, B. B. Lowell, The paraventricular hypothalamus regulates satiety and prevents obesity via two genetically distinct circuits. *Neuron* **102**, 653–667.e6 (2019).
11. H. Pei, A. K. Sutton, K. H. Burnett, P. M. Fuller, D. P. Olson, AVP neurons in the paraventricular nucleus of the hypothalamus regulate feeding. *Mol. Metab.* **3**, 209–215 (2014).
12. N. Balthasar, L. T. Dalgaard, C. E. Lee, J. Yu, H. Funahashi, T. Williams, M. Ferreira, V. Tang, R. A. McGovern, C. D. Kenny, L. M. Christiansen, E. Edelstein, B. Choi, O. Boss, C. Aschkenasi, C. Y. Zhang, K. Mountjoy, T. Kishi, J. K. Elmquist, B. B. Lowell, Divergence of melanocortin pathways in the control of food intake and energy expenditure. *Cell* **123**, 493–505 (2005).
13. J. L. Holder Jr., N. F. Butte, A. R. Zinn, Profound obesity associated with a balanced translocation that disrupts the SIM1 gene. *Hum. Mol. Genet.* **9**, 101–108 (2000).
14. A. Bonnefond, A. Raimondo, F. Stutzmann, M. Ghoussaini, S. Ramachandrappa, D. C. Bersten, E. Durand, V. Vatin, B. Balkau, O. Lantieri, V. Raverdy, F. Pattou, W. van Hul, L. van Gaal, D. J. Peet, J. Weill, J. L. Miller, F. Horber, A. P. Goldstone, D. J. Driscoll, J. B. Bruning, D. Meyre, M. L. Whitelaw, P. Froguel, Loss-of-function mutations in SIM1 contribute to obesity and Prader-Willi-like features. *J. Clin. Invest.* **123**, 3037–3041 (2013).
15. S. Ramachandrappa, A. Raimondo, A. M. G. Cali, J. M. Keogh, E. Henning, S. Saeed, A. Thompson, S. Garg, E. G. Bochukova, S. Brage, V. Trowse, E. Wheeler, A. E. Sullivan, M. Dattani, P. E. Clayton, V. Datta, J. B. Bruning, N. J. Wareham, S. O'Rahilly, D. J. Peet, I. Barroso, M. L. Whitelaw, I. S. Farooqi, Rare variants in single-minded 1 (SIM1) are associated with severe obesity. *J. Clin. Invest.* **123**, 3042–3050 (2013).
16. M. C. Bonaglia, R. Ciccone, G. Gimelli, S. Gimelli, S. Marelli, J. Verheij, R. Giorda, R. Grasso, R. Borgatti, F. Pagone, L. Rodrìguez, M. L. Martinez-Frias, C. van Ravenswaaij, O. Zuffardi, Detailed phenotype-genotype study in five patients with chromosome 6q16 deletion: narrowing the critical region for Prader-Willi-like phenotype. *Eur. J. Hum. Genet.* **16**, 1443–1449 (2008).
17. J. L. Holder Jr., L. Zhang, B. M. Kublaoui, R. J. DiLeone, O. K. Oz, C. H. Bair, Y. H. Lee, A. R. Zinn, Sim1 gene dosage modulates the homeostatic feeding response to increased dietary fat in mice. *Am. J. Physiol. Endocrinol. Metab.* **287**, E105–E113 (2004).
18. J. L. Michaud, F. Boucher, A. Melnyk, F. Gauthier, E. Goshu, E. Lévy, G. A. Mitchell, J. Himms-Hagen, C. M. Fan, Sim1 haploinsufficiency causes hyperphagia, obesity and reduction of the paraventricular nucleus of the hypothalamus. *Hum. Mol. Genet.* **10**, 1465–1473 (2001).
19. S. M. Duplan, F. Boucher, L. Alexandrov, J. L. Michaud, Impact of Sim1 gene dosage on the development of the paraventricular and supraoptic nuclei of the hypothalamus. *Eur. J. Neurosci.* **30**, 2239–2249 (2009).
20. B. M. Kublaoui, T. Gemelli, K. P. Tolson, Y. Wang, A. R. Zinn, Oxytocin deficiency mediates hyperphagic obesity of Sim1 haploinsufficient mice. *Mol. Endocrinol.* **22**, 1723–1734 (2008).
21. B. M. Kublaoui, J. L. Holder Jr., T. Gemelli, A. R. Zinn, Sim1 haploinsufficiency impairs melanocortin-mediated anorexia and activation of paraventricular nucleus neurons. *Mol. Endocrinol.* **20**, 2483–2492 (2006).
22. C. Yang, D. Gagnon, P. Vachon, A. Tremblay, E. Levy, B. Massie, J. L. Michaud, Adenoviral-mediated modulation of Sim1 expression in the paraventricular nucleus affects food intake. *J. Neurosci.* **26**, 7116–7120 (2006).
23. K. P. Tolson, T. Gemelli, L. Gautron, J. K. Elmquist, A. R. Zinn, B. M. Kublaoui, Postnatal Sim1 deficiency causes hyperphagic obesity and reduced Mc4r and oxytocin expression. *J. Neurosci.* **30**, 3803–3812 (2010).
24. K. P. Tolson, T. Gemelli, D. Meyer, U. Yazdani, J. Kozlitina, A. R. Zinn, Inducible neuronal inactivation of Sim1 in adult mice causes hyperphagic obesity. *Endocrinology* **155**, 2436–2444 (2014).
25. S. Smemo, J. J. Tena, K. H. Kim, E. R. Gamazon, N. J. Sakabe, C. Gómez-Marín, I. Aneas, F. L. Credidio, D. R. Sobreira, N. F. Wasserman, J. H. Lee, V. Puviindran, D. Tam, M. Shen, J. E. Son, N. A. Vakili, H. K. Sung, S. Naranjo, R. D. Acemel, M. Manzanares, A. Nagy, N. J. Cox, C. C. Hui, J. L. Gomez-Skarmeta, M. A. Nóbrega, Obesity-associated variants within FTO form long-range functional connections with IRX3. *Nature* **507**, 371–375 (2014).
26. M. Claussnitzer, S. N. Dankel, K. H. Kim, G. Quon, W. Meuleman, C. Haugen, V. Glunk, I. S. Sousa, J. L. Beaudry, V. Puviindran, N. A. Abdennur, J. Liu, P. A. Svensson, Y. H. Hsu, D. J. Drucker, G. Mellgren, C. C. Hui, H. Hauner, M. Kellis, FTO Obesity Variant circuitry and adipocyte browning in humans. *N. Engl. J. Med.* **373**, 895–907 (2015).
27. D. R. Sobreira, A. C. Joslin, Q. Zhang, I. Williamson, G. T. Hansen, K. M. Farris, N. J. Sakabe, N. Sinnott-Armstrong, G. Bozek, S. O. Jensen-Cody, K. H. Flippo, C. Ober, W. A. Bickmore, M. Potthoff, M. Chen, M. Claussnitzer, I. Aneas, M. A. Nóbrega, Extensive pleiotropism and allelic heterogeneity mediate metabolic effects of IRX3 and IRX5. *Science* **372**, 1085–1091 (2021).
28. J. E. Son, Z. Dou, K. H. Kim, S. Wanggou, V. S. B. Cha, R. Mo, X. Zhang, X. Chen, T. Ketela, X. Li, X. Huang, C. C. Hui, Irx3 and Irx5 in Ins2-Cre(+) cells regulate hypothalamic postnatal neurogenesis and leptin response. *Nat. Metab.* **3**, 701–713 (2021).
29. L. Madisen, T. A. Zwingman, S. M. Sunkin, S. W. Oh, H. A. Zariwala, H. Gu, L. L. Ng, R. D. Palmiter, M. J. Hawrylycz, A. R. Jones, E. S. Lein, H. Zeng, A robust and high-throughput

Cre reporting and characterization system for the whole mouse brain. *Nat. Neurosci.* **13**, 133–140 (2010).
30. W. Wang, T. Lufkin, The murine Otp homeobox gene plays an essential role in the specification of neuronal cell lineages in the developing hypothalamus. *Dev. Biol.* **227**, 432–449 (2000).
31. S. Nakai, H. Kawano, T. Yudate, M. Nishi, J. Kuno, A. Nagata, K. Jishage, H. Hamada, H. Fujii, K. Kawamura, The POU domain transcription factor Brn-2 is required for the determination of specific neuronal lineages in the hypothalamus of the mouse. *Genes Dev.* **9**, 3109–3121 (1995).
32. M. D. Schonemann, A. K. Ryan, R. J. McEvilly, S. M. O'Connell, C. A. Arias, K. A. Kalla, P. Li, P. E. Sawchenko, M. G. Rosenfeld, Development and survival of the endocrine hypothalamus and posterior pituitary gland requires the neuronal POU domain factor Brn-2. *Genes Dev.* **9**, 3122–3135 (1995).
33. F. Liu, Y. Zhang, L. Zhang, Z. Li, Q. Fang, R. Gao, Z. Zhang, Systematic comparative analysis of single-nucleotide variant detection methods from single-cell RNA sequencing data. *Genome Biol.* **20**, 242 (2019).
34. C. Ziegenhain, B. Vieth, S. Parekh, B. Reinius, A. Guillaumet-Adkins, M. Smets, H. Leonhardt, H. Heyn, I. Hellmann, W. Enard, Comparative analysis of single-Cell RNA sequencing methods. *Mol. Cell* **65**, 631–643.e4 (2017).
35. D. Li, R. Sakuma, N. A. Vakili, R. Mo, V. Puviindran, S. Deimling, X. Zhang, S. Hopyan, C. C. Hui, Formation of proximal and anterior limb skeleton requires early function of Irx3 and Irx5 and is negatively regulated by Shh signaling. *Dev. Cell* **29**, 233–240 (2014).
36. N. Matharu, S. Rattanasopha, S. Tamura, L. Maliskova, Y. Wang, A. Bernard, A. Hardin, W. L. Eckalbar, C. Vaisse, N. Ahituv, CRISPR-mediated activation of a promoter or enhancer rescues obesity caused by haploinsufficiency. *Science* **363**, eaau0629 (2019).
37. E. J. Bellefroid, A. Kobbe, P. Gruss, T. Pieler, J. B. Gurdon, N. Papalopulu, Xiro3 encodes a Xenopus homolog of the Drosophila Iroquois genes and functions in neural specification. *EMBO J.* **17**, 191–203 (1998).
38. J. L. Gomez-Skarmeta, A. Glavic, E. de la Calle-Mustienes, J. Modolell, R. Mayor, Xiro, a Xenopus homolog of the Drosophila Iroquois complex genes, controls development at the neural plate. *EMBO J.* **17**, 181–190 (1998).
39. F. Cavodeassi, J. Modolell, J. L. Gomez-Skarmeta, The Iroquois family of genes: from body building to neural patterning. *Development* **128**, 2847–2855 (2001).
40. D. R. Cohen, C. W. Cheng, S. H. Cheng, C. C. Hui, Expression of two novel mouse Iroquois homeobox genes during neurogenesis. *Mech. Dev.* **91**, 317–321 (2000).
41. D. E. G. McNay, M. Pelling, S. Claxton, F. Guillemot, S.-L. Ang, Mash1 is required for generic and subtype differentiation of hypothalamic neuroendocrine cells. *Mol. Endocrinol.* **20**, 1623–1632 (2006).
42. G. Alvarez-Bolado, Development of neuroendocrine neurons in the mammalian hypothalamus. *Cell Tissue Res.* **375**, 23–39 (2019).
43. C. Li, J. Navarrete, J. Liang-Guallpa, C. Lu, S. C. Funderburk, R. B. Chang, S. D. Liberles, D. P. Olson, M. J. Krashes, Defined paraventricular hypothalamic populations exhibit differential responses to food contingent on caloric state. *Cell Metab.* **29**, 681–694.e5 (2019).
44. J. Biran, M. Tahor, E. Wircer, G. Levkowitz, Role of developmental factors in hypothalamic function. *Front. Neuroanat.* **9**, 47 (2015).
45. S. Feng, C. Xing, T. Shen, Y. Qiao, R. Wang, J. Chen, J. Liao, Z. Lu, X. Yang, S. M. Abd-Allah, J. Li, N. Jing, K. Tang, Abnormal paraventricular nucleus of hypothalamus and growth retardation associated with loss of nuclear receptor gene COUP-TFII. *Sci. Rep.* **7**, 5282 (2017).
46. J. Z. Kiss, Anatomical studies of cholecystokinin in neurons and pathways involved in neuroendocrine regulation. *Ann. N. Y. Acad. Sci.* **448**, 144–151 (1985).
47. M. Bulbul, O. Sinen, L. Abueid, G. Akkoyunlu, O. Ozsoy, Central apelin administration and restraint stress induce hypothalamic cholecystokinin release via the APJ receptor. *J. Neuroendocrinol.* **30**, e12635 (2018).
48. C. F. Elias, C. E. Lee, J. F. Kelly, R. S. Ahima, M. Kuhar, C. B. Saper, J. K. Elmquist, Characterization of CART neurons in the rat and human hypothalamus. *J. Comp. Neurol.* **432**, 1–19 (2001).
49. L. Peter, A. Stengel, S. Noetzel, T. Inhoff, M. Goebel, Y. Taché, R. W. Veh, N. Bannert, C. Grötzinger, B. Wiedenmann, B. F. Klapp, H. Mönnikes, P. Kobelt, Peripherally injected CCK-8S activates CART positive neurons of the paraventricular nucleus in rats. *Peptides* **31**, 1118–1123 (2010).
50. J. F. Marion, C. Yang, A. Caqueret, F. Boucher, J. L. Michaud, Sim1 and Sim2 are required for the correct targeting of mammillary body axons. *Development* **132**, 5527–5537 (2005).
51. S. S. Zhang, K. H. Kim, A. Rosen, J. W. Smyth, R. Sakuma, P. Delgado-Olguin, M. Davis, N. C. Chi, V. Puviindran, N. Gaborit, T. Sukonnik, J. N. Wylie, K. Brand-Arzamendi, G. P. Farman, J. Kim, R. A. Rose, P. A. Marsden, Y. Zhu, Y. Q. Zhou, L. Miquerol, R. M. Henkelman, D. Y. R. Stainier, R. M. Shaw, C. C. Hui, B. G. Bruneau, P. H. Backx, Iroquois homeobox gene 3 establishes fast conduction in the cardiac His-Purkinje network. *Proc. Natl. Acad. Sci. U.S.A.* **108**, 13576–13581 (2011).
52. E. Z. Macosko, A. Basu, R. Satija, J. Nemesh, K. Shekhar, M. Goldman, I. Tirosh, A. R. Bialas, N. Kamitaki, E. M. Martersteck, J. J. Trombetta, D. A. Weitz, J. R. Sanes, A. K. Shalek, A. Regev, S. A. McCarroll, Highly parallel genome-wide expression profiling of individual cells using nanoliter droplets. *Cell* **161**, 1202–1214 (2015).
53. A. Dobin, C. A. Davis, F. Schlesinger, J. Drenkow, C. Zaleski, S. Jha, P. Batut, M. Chaisson, T. R. Gingeras, STAR: Ultrafast universal RNA-seq aligner. *Bioinformatics* **29**, 15–21 (2013).
54. A. Butler, P. Hoffman, P. Smibert, E. Papalexi, R. Satija, Integrating single-cell transcriptomic data across different conditions, technologies, and species. *Nat. Biotechnol.* **36**, 411–420 (2018).
55. J. N. Campbell, E. Z. Macosko, H. Fenselau, T. H. Pers, A. Lyubetskaya, D. Tenen, M. Goldman, A. M. J. Verstegen, J. M. Resch, S. A. McCarroll, E. D. Rosen, B. B. Lowell, L. T. Tsai, A molecular census of arcuate hypothalamus and median eminence cell types. *Nat. Neurosci.* **20**, 484–496 (2017).
56. J. J. An, C. E. Kinney, J. W. Tan, G. Y. Liao, E. J. Kremer, B. Xu, TrkB-expressing paraventricular hypothalamic neurons suppress appetite through multiple neurocircuits. *Nat. Commun.* **11**, 1729 (2020).
57. C. C. Hui, A. L. Joyner, A mouse model of greig cephalopolysyndactyly syndrome: The extra-toesJ mutation contains an intragenic deletion of the Gli3 gene. *Nat. Genet.* **3**, 241–246 (1993).
58. A. Jandura, J. Hu, R. Wilk, H. M. Krause, High resolution fluorescent in situ hybridization in drosophila embryos and tissues using tyramide signal amplification. *J. Vis. Exp.* **2017**, 56281 (2017).

Acknowledgments: We thank T. Ketela at the Princess Margaret Genomics Centre for assisting the scRNA-seq analysis. **Funding:** The research was supported by Canadian Institutes of Health Research (MOP-136821) and the Canada Research Chairs program to C.-c.H. J.E.S. was supported by a postdoctoral fellowship award from Diabetes Canada. J.E.S. was awarded a Basic Science Research Program through the National Research Foundation of Korea (NRF) funded by the Ministry of Education (2018R1A6A3A03012237). **Author contributions:** J.E.S., X.L., X.H., K.K.H., J.L.M., and C.-c.H. conceived and designed the study. J.E.S. and J.C. performed the mouse experiments. J.E.S. and R.M., carried out the RNA and protein analyses. J.E.S., Z.D., and S.W., performed the scRNA-seq analysis. J.E.S. and C.-c.H. wrote the manuscript with input from all authors. **Competing interests:** The authors declare that they have no competing interests. **Data and materials availability:** All data needed to evaluate the conclusions in the paper are present in the paper and/or the Supplementary Materials. Drop-seq data have been deposited in Gene Expression Omnibus (GEO) under accession code GSE166616. The *Irx3*^{tauLacZ} mice, *Irx5*^{eGFP} mice, *Irx3*$^{-}$*5*^{eGFP} mice, and *Irx3*-floxed (*Irx3*^{Flox}) mice can be provided by C.-c.H. pending scientific review and a completed material transfer agreement. Requests for the *Irx3*^{tauLacZ} mice, *Irx5*^{eGFP} mice, *Irx3*$^{-}$*5*^{eGFP} mice, and *Irx3*-floxed (*Irx3*^{Flox}) mice should be submitted to C.-c.H. The *Sim1*^{tLZ} (*Sim1*^{Het}) mice can be provided by J.L.M. pending scientific review and a completed material transfer agreement. Requests for the *Sim1*^{Het} mice should be submitted to J.L.M.

Submitted 11 March 2021
Accepted 3 September 2021
Published 27 October 2021
10.1126/sciadv.abh4503

Citation: J. E. Son, Z. Dou, S. Wanggou, J. Chan, R. Mo, X. Li, X. Huang, K.-H. Kim, J. L. Michaud, C.-c. Hui, Ectopic expression of *Irx3* and *Irx5* in the paraventricular nucleus of the hypothalamus contributes to defects in *Sim1* haploinsufficiency. *Sci. Adv.* **7**, eabh4503 (2021).